

Prussian Blue-doped RGO/Mxene Composite Aerogel With Peroxidase-like Activity for Real-time Monitoring H₂O₂ Secretion From Living Cells

Peng Zhao^a, Yuanyuan Jia^a, Yi Liang^a, Jilin Zheng^a, Danqun Huo^{a,b}, Yongzhong Wang^{a*}, Changjun Hou^{a,c*}

^a Key Laboratory for Biorheological Science and Technology (Chongqing University), Ministry of Education, College of Bioengineering, Chongqing University, Chongqing 400044, PR China

^b Chongqing Key Laboratory of Bio-perception & Intelligent Information Processing, School of Microelectronics and Communication Engineering, Chongqing University, Chongqing, 400044, PR China

^c National Facility for Translational Medicine, Shanghai Jiao Tong University, Shanghai, 200240, PR, China

* Corresponding author.

E-mail addresses: wangyzh@cqu.edu.cn; houcj@cqu.edu.cn

Contents

- S1. Materials and instruments**
- S2. Fabrication of 3D PB/GMA**
- S3. Construction of electrochemical sensor**
- S4. Cell culture and drug stimulation**
- S5. DFT simulations**
- S6. TEM images of Mxene nanosheets**
- S7. XPS spectrum of 3D PB/GMA**
- S8. DFT calculation**
- S9. The photograph of formed 3D GMA using different reductants**
- S10. CVs obtained in 0.1 M KCl+5 mM [Fe(CN)₆]^{3-/4-}**
- S11. Current responses obtained at different set conditions**
- S12. Performances of some H₂O₂ electrochemical sensors**
- S13. Reproducibility and stability of the sensor**
- S14. Evaluation of the biocompatibility of 3D PB/MGA**

S1. Materials and instruments

Ti₃AlC₂ was acquired from 11 technology Co., Ltd (Jilin, China). Ascorbic acid (AA), uric acid (UA), L-cysteine (L-Cys), NH₃·H₂O and N₂H₄·H₂O, dopamine hydrochloride (DA), glutamine (Gln) and phorbol-12-myristate-13-acetate (PMA) were purchased from Sigma-Aldrich (Shanghai, China). Hydrogen peroxide (H₂O₂), and Glucose (Glu) were purchased from Chongqing Chuan Dong Chemical Group (China). 3',6'-di(oacetyl)-4',5'-bis[N,N-bis(carboxymethyl)amino-methyl] fluorescein, tetraacetoxyme-thylester (Calcein-AM), and 3,8-diamino-5-[3-(diethylmethylammonio)propyl]-6-phenylphenanthridinium diiodide (PI) were bought from Solarbio Science &Technology Co., Ltd (Beijing, China).

The morphologies characterization was performed on field-emission scanning electron microscope (FESEM, JEOL-6300F) and transmission electron microscope (TEM, Talos F200S). The chemical composition were surveyed by X-ray photoelectron spectroscopy (ESCALAB 250Xi, ThermoFisher). Electrochemical tests including cyclic voltammetry (CV), and amperometric i-t curve were performed on a CHI 660E electrochemical workstation (Shanghai CH Instrument, China). An

inverted fluorescent microscope (DM IL LED, Leica, Germany) was used for fluorescence imaging.

S2. Fabrication of 3D PB/GMA

Firstly, Ti_3C_2 Mxene nanosheets were synthesized according to previous report¹. Briefly, 2 g of LiF was dissolved in 40 mL of HCl (9 M), then 2 g of Ti_3AlC_2 was appended and kept stirring for 24 h at 35°C. The obtained suspension was centrifuged at 3500 rpm and washed with deionized water (until pH~7). Then, the sediment was dispersed in distilled water under the protection of Ar.

3D PB/GMA was fabricated through one-step self-assembly method (Fig. S1). Typically, 2 mL of Ti_3C_2 Mxene colloidal suspension (2 mg mL^{-1}) and 2 mL of GO suspension (2 mg mL^{-1}) were fully mixed by ultrasound. After that, 0.0741 g $\text{K}_3[\text{Fe}(\text{CN})_6]$ and 0.0609 g $\text{FeCl}_3 \cdot 6\text{H}_2\text{O}$ were added and continued to sonicate for 15 min. Then, 10 μL EDA solution was injected and the mixture was treated at 90 °C for 6 h to form 3D PB NPs/MGH. The obtained hydrogel was thoroughly immersed in deionized water to remove residual molecules, followed by freeze-dried for 24 h. For comparison, reductant AA was also used.

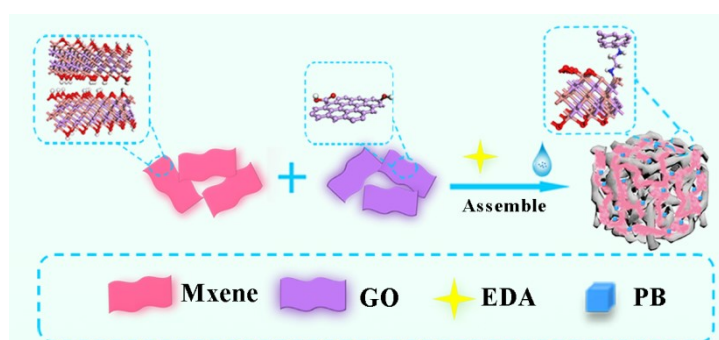


Fig. S1 Schematic illustration of self-assembly of 3D PB/GMA.

S3. Construction of electrochemical sensor

The electrochemical sensor is constructed based on three-electrode system. Glassy carbon electrode (GCE) modified with composite aerogel was used as the working electrode. An Ag/AgCl electrode and the Pt mesh were used as the reference electrode and the counter electrode, respectively. Phosphate buffered saline (0.01 M, pH 7.4) solution was used as the electrolyte. The GCE was firstly polished with alumina slurries and cleaned with ethanol and deionized water. Then, 5 μL of 3D PB/GMA dispersion was modified onto the cleaned GCE and dried to form 3D PB/GMA@GCE.

S4. Cell culture and drug stimulation

Living cells were maintained in DMEM/F-12 (Hyclone, USA) supplemented with 10% fetal bovine serum (FBS) and 1% penicillin-streptomycin (P/S) solution at 37°C with 5% CO₂ in a 95% humidified atmosphere. After growing to ~90% confluence, the cells were collected and resuspended into 10 mL PBS (PH=7.4) solution with a density of $\sim 5 \times 10^5$ cells mL⁻¹. PMA was applied to trigger cells to produce H₂O₂. Meanwhile, catalase was used to test the specificity of secretory H₂O₂.

S5. DFT simulations

To better understand the formation mechanism and configuration characteristic, DFT was performed on CASTEP program. For geometry optimization, PW91 function with generalized gradient approximation (CGA) was employed to deal with the electron exchange and correlation², and TS DFT-D3 method was used for the correction of van der vaals interaction³. The Monkhorst–Pack k-point grids were set to 5×5×1. The cutoff energy was performed on 500 eV. And a convergence of 10⁻⁶ eV/atom was used for self-consistent field (SCF) computation.

S6. TEM images of Mxene nanosheets

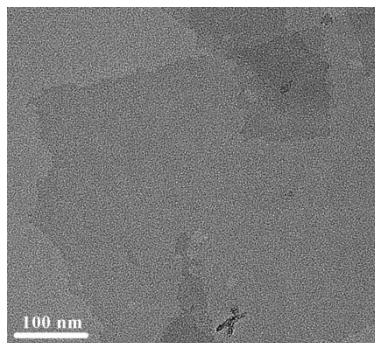


Fig. S2 TEM images of Mxene nanosheets.

S7. XPS spectrum of 3D PB/GMA

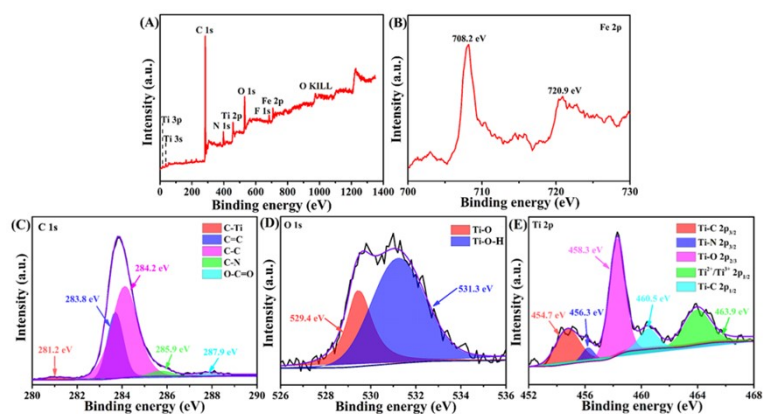


Fig. S3 XPS spectrum of 3D PB/GMA: (A) Survey; (B) Fe 2p; (C) C 1s; (D) O 1s; (E) Ti 2p.

S8. DFT calculation

To save computation resources, a $3 \times 3 \times 1$ supercell of reduced graphene oxide modified with EDA (EDA-RGO) and $3 \times 3 \times 1$ supercell of Ti_3C_2 modified with -O-groups were constructed and optimized. The binding energies (E_b) was calculated by such a formula:

$$E_b = E_{EDA-RGO} - (E_{RGO} + E_{EDA}) \quad (1)$$

where $E_{EDA-RGO}$, E_{RGO} , and E_{EDA} mean the total energies of the optimized EDA-RGO, RGO, and EDA, respectively.

To better understand the formation mechanism between EDA-RGO and Ti_3C_2 , density functional theory (DFT) was performed. The side and top view of optimized RGO, EDA-RGO and $\text{Ti}_3\text{C}_2\text{O}_x$ structures are presented in Fig. S4A. Herein, EDA can firstly bind to RGO through strong chemical bond (C-N bond) during the reduction process. The binding energies between RGO and EDA is about 1.15 eV, indicating a strong interaction. In electron density difference map (Fig. S4B), EDA-RGO shows an electron-deficient in carbon plane and electron enrichment in amino group. And Ti_3C_2 present an obvious electron-deficient in marginal Ti atom, which could act as an electron acceptor. From the perspective of mutual interactions, a nucleophilic attack would take place from N atom in formed EDA-RGO to marginal Ti atom in Ti_3C_2 . Thus, the Ti-N coordination bands are formed, which promotes strong interactions between the two components. This result is well consist with Ti 2p XPS spectrum. Driven by supramolecular forces, the hybrid aerogel is obtained (Fig. S4C). And such hybrid aerogel formation mechanism was further confirmed by experiment using

other reductants including L-cysteine, $\text{NH}_3\cdot\text{H}_2\text{O}$ and $\text{N}_2\text{H}_4\cdot\text{H}_2\text{O}$ (Fig. S5), which can functionalize RGO with amino groups.

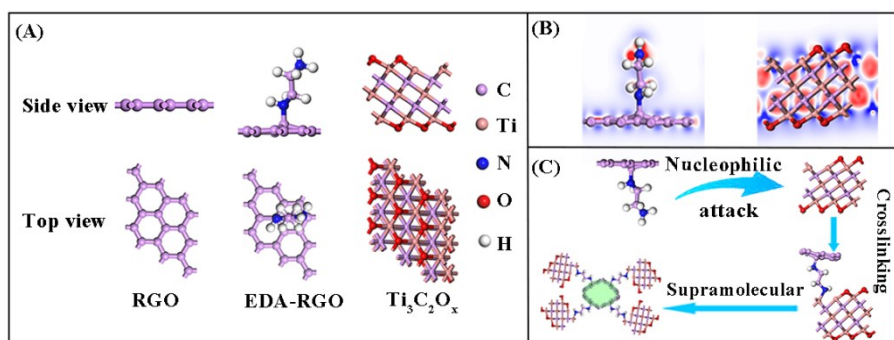


Fig. S4 (A) Side and top view of optimized structure models. (B) Electron density difference map of EDA-RGO and Mxene. Red and blue represent electron enrichment and deficient, respectively. (C) Illustration of the possible formation mechanism of the aerogel.

S9. The photograph of formed 3D GMA using different reductant

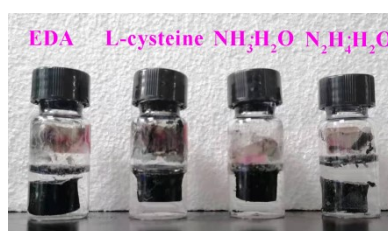


Fig. S5 The photograph of formed gel using different reductants.

S10. CVs obtained in 0.1 M KCl+5 mM $[\text{Fe}(\text{CN})_6]^{3-/4-}$

To evaluate the electrochemical property, cyclic voltammetry curves was performed in 0.1 M KCl containing 5 mM $[\text{Fe}(\text{CN})_6]^{3-/4-}$. As observed in Fig. S6, the original electrode exhibits a pair of favorable redox curve. After GMA modification, the redox peaks enlarges greatly, indicating that GMA can strengthen the electroconductivity significantly. Further functionalization with PB nanoparticles leads to further enhanced redox peak. The synergistic action of GMA and PB nanoparticles promises the excellent electrochemical property. Besides, the superior current intensity of 3D PB/GMA indicates a promising charge transferability. For this reason, 3D PB/GMA shows a good application ability for electrochemical sensing.

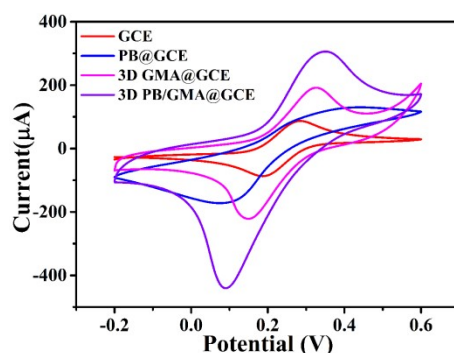


Fig. S6 CVs obtained in 0.1 M KCl+5 mM $[\text{Fe}(\text{CN})_6]^{3-/4-}$. Scan rate: 0.05 V s⁻¹.

S11. Current responses obtained at different set conditions

To better evaluate the sensing performance, two experimental parameters including applied potential and aerogel loading volume were optimized. As show in Fig. S7A, the current responses steadily enhances and reaches a supreme value at -0.4 V. Fig. S7B presents the influence of aerogel loading volume on sensing performance. With the loading volume rises to 5 μL , the greatest current response is obtained.

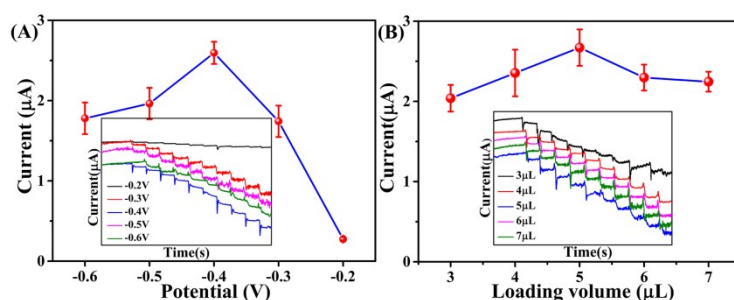


Fig. S7 Current responses obtained at different set conditions: (A) the applied potential; (B) 3D PB/GMA loading volume.

S12. Performances of some H_2O_2 electrochemical sensors

Table 1 Performances of some H_2O_2 electrochemical sensors.

Electrode material	Linear range (μM)	LOD (μM)	Application	Ref
Pt-Pd/CFME	5-3920	0.42	A549 cells	4
CNT/graphene/MnO	7-25000	6.7	Hep2 cells	5
ZnMn ₂ O ₄ @rGO	0.03-6000	0.012	MCF-7 cells	6

MoS ₂ /CC	5-235	1.0	A549 cells	7
pFeMOF/OMC	0.5-70.5	0.45	HeLa cells	8
3D PB/GMA	0.1-300	0.028	HBL-100 cells	this work
			A549 cells	
			MCF-7 cells	

S13. Reproducibility and stability of the sensor

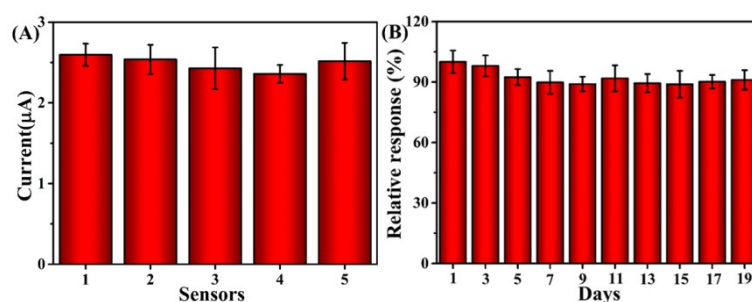


Fig. S8 (A) Current responses obtained at five individual sensors. (B) Relative responses over 19 days.

S14. Evaluation of the biocompatibility of 3D PB/MGA

The biocompatibility of 3D PB/MGA was evaluated by standard staining method. Herein, one normal cell line (HBL-100 cells) and one cancer cell line (MCF-7 cells) were used as the model, which were incubated with 3D PB/MGA (8 µg/mL) for 24 h and then stained by fluorescent live/dead cell markers (Calcein-AM and PI). As observed in Fig. S9, these cells still present a good morphology and viability after long-term incubation with 3D PB/MGA, indicating a good biocompatibility of the hybrid aerogel.

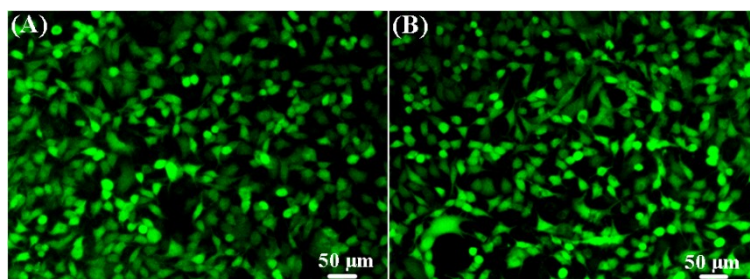


Fig. S9 Fluorescence imagings of (A) HBL-100 cells and (B) MCF-7 cells cultured with 3D PB/MGA for 24 h and labeled with Calcein-AM and PI.

References

- 1 Ji, C.; Wang, Y.; Ye, Z.; Tan, L.; Mao, D.; Zhao, W.; Zeng, X.; Yan, C.; Sun, R.; Kang, D. J.; Xu, J.; Wong, C.-P., *ACS Appl. Mater. Interfaces*, 2020, **12**, 24298-24307.
- 2 Shang, T.; Lin, Z.; Qi, C.; Liu, X.; Li, P.; Tao, Y.; Wu, Z.; Li, D.; Simon, P.; Yang, Q.-H., *Adv. Funct. Mater.*, 2019, **29**.
- 3 Perdew, J. P.; Burke, K.; Ernzerhof, M., *Phys. Rev. Lett.*, 1996, **77**, 3865-3868.
- 4 H. Li, H. Zhao, H. He, L. Shi, X. Cai, M. Lan, *Sens. Actuators, B*, 2018, **260**, 174-182.
- 5 Z. Shi, X. Wu, L. Gao, Y. Tian, L. Yu, *Anal. Methods*, 2014, **6**, 4446-4454.
- 6 Y. Li, K. Huan, D. Deng, L. Tang, J. Wang, L. Luo, *ACS Appl. Mater. Interfaces*, 2019, **12**, 3430-7.
- 7 H. Du, X. Zhang, Z. Liu, F. Qu, *Chem. Commun.*, 2019, **55**, 9653-9656.
- 8 J. Liu, X. Bo, J. Yang, D. Yin, L. Guo, *Sens. Actuators, B*, 2017, **248**, 207-213.